Light Metals 2013 *Edited by: Barry Sadler*
TMS (The Minerals, Metals & Materials Society), 2013

The Challenge of Effectively Utilizing Trace Elements/Impurities in a Varying Raw Materials Market

Gyan Jha[1], Shridas Ningileri[2], Xiaoxuan Li[2], Randall Bowers[2]
[1]Tri-Arrows Aluminum, 9960 Corporate Campus Dr, Suite 3000, Louisville, KY 40223
[2]SECAT, Inc., 1505 Bull Lea Rd, Lexington, KY 40511

Keywords: Aluminum, Vanadium, Coke, Anode, Direct Chill (DC), Thermo-Calc

Abstract

As technology and innovation advances, so do the materials which we use, and in turn, the raw material stream is continually impacted. Today, plants are faced with the challenge of ideally capitalizing on the positive benefits of trace elements when they exist, or following in previous paths of tolerating the increased levels of the elements, and in the worst case, removing the elements at a large expense in production costs. Presented are recent trends observed for various elements, their origins within the raw material stream, and discussions of the need to reexamine how trace elements are handled today and in the future. What is tolerable in certain aluminum alloy products and potential benefits in properties will be explored in addition to the challenges required to remove the elements effectively when needed.

Introduction

Primary aluminum production through the Hall-Heroult process introduces impurities through a variety of pathways into the aluminum stream. Whether in the alumina, the electrolyte, or the anode, these impurities ultimately will collect into the prime from the smelting process (1). One example of increased impurity content in the smelting is the aluminum alloy trace elements of nickel (Ni) and vanadium (V), which increasingly have been found to contaminate the petroleum coke used for manufacture of anodes. The consequence of the Ni and V contamination is an increase in levels for the downstream alloys produced using prime sources. In these alloys, understanding the role of the trace elements, their impact and mitigation strategies in the alloy production are vital to producing a low cost, high quality product. Discussed in the following paper is an example methodology to determine impact of low level trace elements in a controlled manner so that these increases don't produce a diminishing return on alloy performance and at the same time lowering raw material costs by using lower grade prime.

Methodology

As raw material inputs is one of the main costs associated with aluminum alloy production, a concerted effort was made to understand the market availability of prime at varying grades and to develop a strategy for forecasting impurity levels. Impurities were grouped as those most expected to increase significantly over the next several years and those expected to remain constant. Those impurities, for which increases were expected, were then selected to be used for experimental trials to determine tolerable levels and any unexpected benefits in allowing the trace specification upper limit to rise for a given element. In the following case study, V was chosen to explore the potential impacts on an AA3xx4 as the V levels were forecasted to reach levels of 600 ppm in future prime production (1). The current V upper limit for this alloy in production is 300 ppm.

The method used in determining the allowable limit for vanadium and the potential impacts first consisted of examining the physical metallurgy of the impurity in aluminum and specifying a level below which are known to negatively affect the finished product. In this way, a realistic upper limit was concluded as not to pose product performance issues a priori based on established findings. Review of published literature, internal reports and practices, thermodynamic equilibrium calculations, and recovery expectations, led to a feasible upper limit which was determined with the forecasted prime impurity content of 600 ppm and an additional amount to cover variability and expected increases within the overall raw material strategy including hardeners, recycled scrap ingot (RSI), etc. Once a suitable limit was established, an experimental alloy with the upper limit of vanadium was produced to examine the overall impact of the impurity and confirm product performance.

Experimental

Two small scale Direct Chill (DC) casts were made – one with standard AA3xx4 chemistry representing current production and one with AA3xx4 chemistry with 0.11 wt. % V representing the highest level anticipated for the alloy in the current raw materials market. Each cast produced two ingots of 6" x 18" x 110". The following table is the ICP assay of the ingots S3xx4 and S3xx4V in weight percent (wt. %).

Table 1: Ingot Chemistry in Wt. %

Element	S3xx4	S3xx4V
Cu	0.17	0.18
Fe	0.59	0.58
Mg	1.08	1.02
Mn	0.89	0.88
Si	0.27	0.24
V	< 0.01	0.11

The ingots were homogenized, hot rolled to re-roll gauge of 0.10" followed by cold rolling to final gauges of 0.01". Recovery heat treatments were performed on the final gauge sheet to duplicate current industrial practice and properties.

Samples of the ingot, re-roll gauge, and finish gauge were analyzed by optical and electron microscopy techniques as well as physical testing to compare for differences. The standard alloy and the experimental alloy were compared in terms of grain structure, constituent particles, precipitation phases, and tensile properties.

Results

Equilibrium Calculations

As a first step in determining the feasibility of the experimental alloy, the computational thermodynamics package Thermo-Calc was used to determine information regarding changes in solidification and stable phases that could occur in the new alloy. Using the Thermotech Al-Data ver.5 database, both Scheil calculations and phase diagrams were made. The Scheil model indicated for the standard and experimental alloy, there would be only minor differences in the temperatures at which phases

formed during solidification, however, there were no new phases predicted to occur over that of the standard alloy. In the table below, the temperatures for both alloys at which phases were predicted to form are shown. The differences are negligible. In addition, the calculated equilibrium temperatures of the phases are shown in the first column using the S3xx4V chemistry for reference.

Table 2: Scheil Solidification Results

Equilibrium Temp., [°C]	Phase	S3xx4 Temp., [°C]	S3xx4V Temp., [°C]
	Liquid	651.0	652.0
652	Matrix (FCC_A1)	650.4	651.7
649	Al_6Mn	648.3	648.8
633	Al_3Fe	631.2	631.3
633	Al(Fe,Mn)Si	624.1	624.0
367	Mg_2Si	587.2	587.2

Using the base chemistry of the S3xx4V alloy and allowing the V to vary from 0.0 - 0.2 wt. %; a phase diagram was constructed using Thermo-Calc. The phase diagram shown in figure 1 indicated the equilibrium phases present for various temperatures during the homogenization, hot working and cold working regions.

Within the homogenization and hot rolling region of 450-600 °C, only one set of phases are at equilibrium for both alloys. Namely, these phases are the Al_6Mn and Al(Fe,Mn)Si. However, upon final hot rolling and coiling at 300-370 °C, the two alloys would have two different sets of equilibrium phases. In the standard alloy S3xx4, the phases of Al_6Fe, Al(Fe,Mn)Si, and Mg_2Si phases would be at equilibrium; for the experimental alloy, S3xx4V, there appears an additional phase, Al_3Fe, to the equilibrium phases of S3xx4. The effect of V is anticipated to stabilize the phase at higher temperatures based on the diagram in figure 1. At temperatures below 300 °C, again, there exists a difference between the equilibrium phases predicted between the two alloys. For the experimental alloy, there is an additional phase, Al_3M $D0_{22}$, which does not exist in the portion of the phase diagram representing the standard alloy without V additions. The Al_3M $D0_{22}$ phase represents a binary phase of Al_3V with a tetragonal structure (2), (3) which would be expected to be coherent to matrix. In the phase, V can substitute with other with elements such as Mn but also Sc, Ti, and Zr substituting as well if they were present (4), (5).

Equilibrium calculations indicate the Al_3V phase would begin to form at 238 °C with a composition of 64.38 wt. % Al – 38.62 wt. % V. At 150 °C, the equilibrium mole fraction for the Al_3V phase is 528 ppm. Only minor amounts of Mn are expected to substitute into the phase Al_3V with concentrations ranging from 9-63 ppm Mn in the temperature range of 150-238 °C. Based on the thermodynamic analysis, a different phase of Al_3V is expected to form in the experimental alloy which is not present in the standard alloy. This expectation does not account for the kinetics of the precipitation for such a compound; only indicating the phase is possible to form at equilibrium.

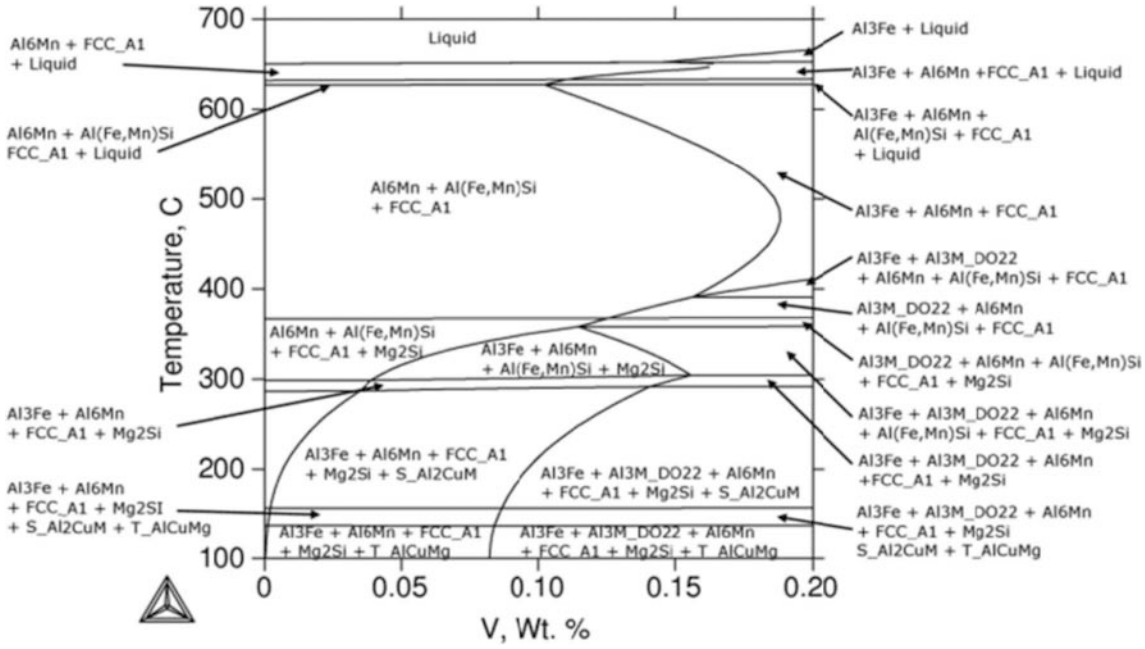

Figure 1: S3xxx4-V Phase Diagram

Constituent Particle Structure

The particle structure of the ingot was characterized by examining across the thickness and width of the ingot slices obtained. Figures 2a and 2b show scanning electron microscope (SEM) images of the particle structures for the two ingots S3xx4 and S3xx4V, respectively. Analysis of the particle structures indicated there was no distinguishable difference to the standard alloy ingot. Energy dispersive spectroscopy (EDS) analysis of the particles confirmed the constituents formed in the ingots were the $Al_6(Fe,Mn)$ and the Mg_2Si phases for both alloys. Vanadium could not be identified in either the particles or the matrix using EDS.

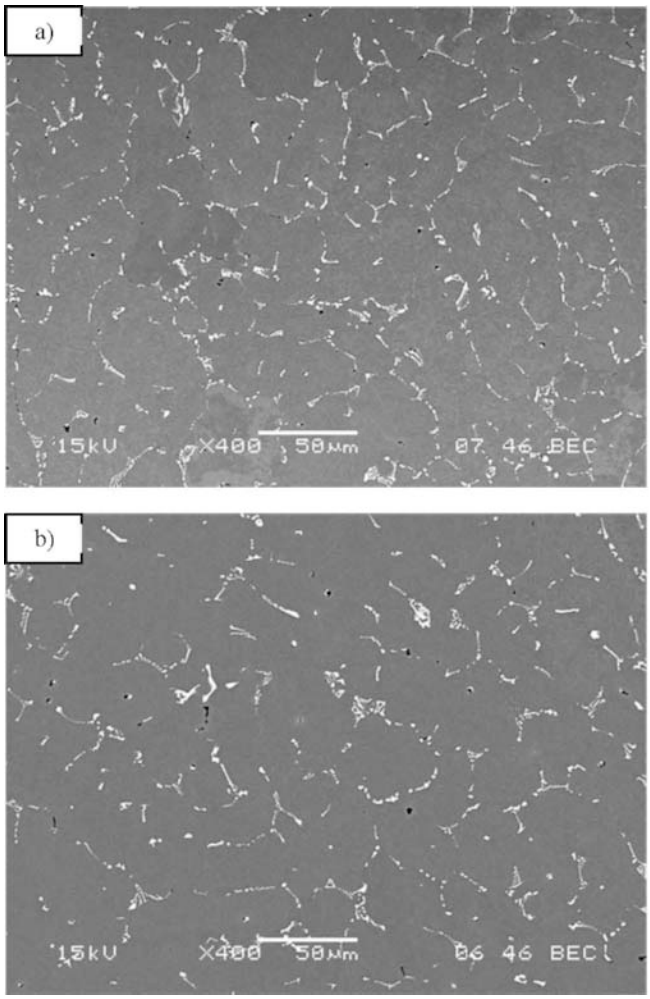

Figure 2: SEM Images of Ingot Particle Structures

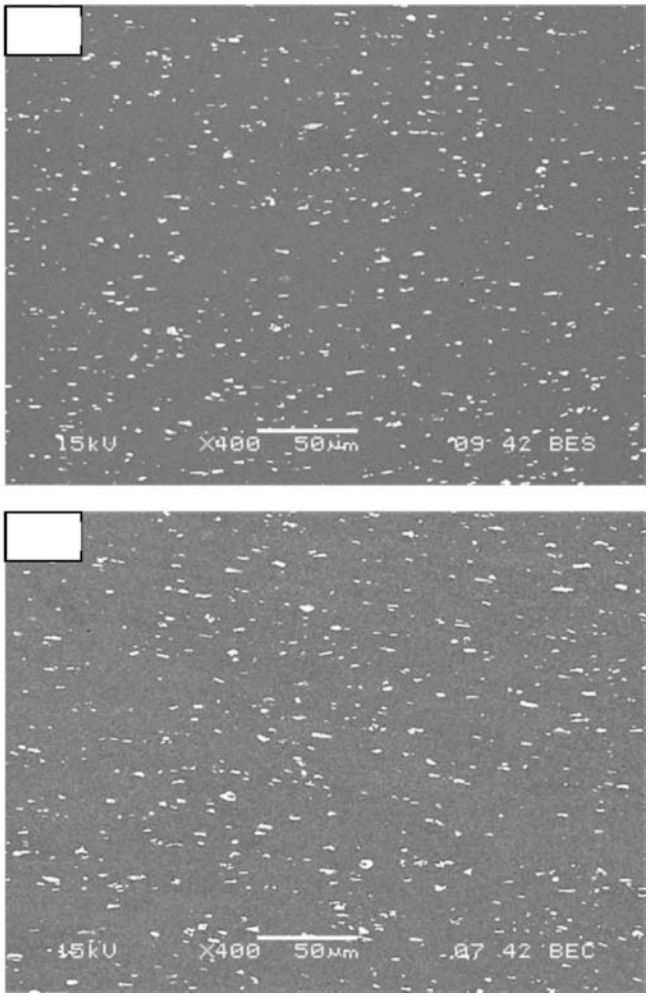

Figure 3: Re-roll Gauge Particle Structures

Samples of re-roll and finish gauge were also examined for particle structure which is shown in figure 3a and 3b for the standard and experimental alloys respectively. The re-roll gauge particle structures were finer as compared to the as-cast structure as expected from the severe deformation in hot rolling. No readily observable difference was seen by image analysis of particle sizes for the two alloys. Finish gauge particle structure investigations yielded similar results.

Grain Structure

The ingot grain structure is shown in figures 4a and 4b for S3xx4 and S3xx4V, respectively. Comparing the grain structures of the two alloys, there were no major differences observed between the two alloys. Both alloys had grain sizes of approximately 300 µm.

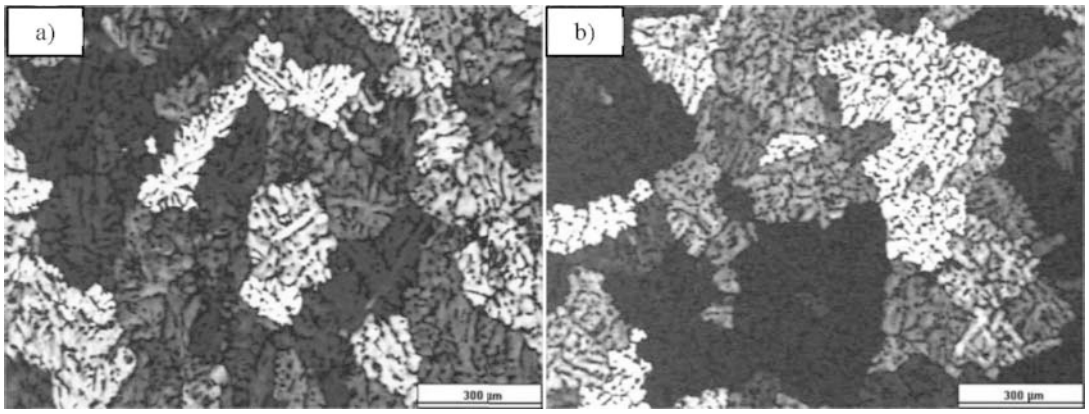

Figure 4: Ingot Grain Structures

At re-roll gauge, the two alloys were again compared for differences in grain structure. The standard alloy grain structure consisted of recrystallized grains, elongated along the rolling direction which is shown in figure 5a. At this stage however, the S3xx4V alloy showed a drastic difference to the grain structure in the standard alloy as seen in figure 5b. The S3xx4V alloy had a much finer recrystallized grain structure which suggests there is an influence on recrystallization for vanadium in the alloy. The grains have an elongated structure along the rolling direction however the length of the elongation is approximately 10% of the length observed for the standard alloy. The through thickness size as well, is approximately half of the through thickness size for the standard alloy. The two alloys had identical thermomechanical histories highlighting the influence of vanadium is evident. Finish gauge grain structures (not shown) only indicated minor differences in grain size in the thickness direction (6).

The lack of differences observed in the particle structures of figure 3a and b indicates the influence of vanadium is likely in the submicron particles that may form (7). A slight modification of phases which would be present in the S3xx4V alloy was predicted by the thermodynamic calculations. Submicron particles would likely be efficient at pinning subgrain boundaries during recrystallization of the cooling coils.

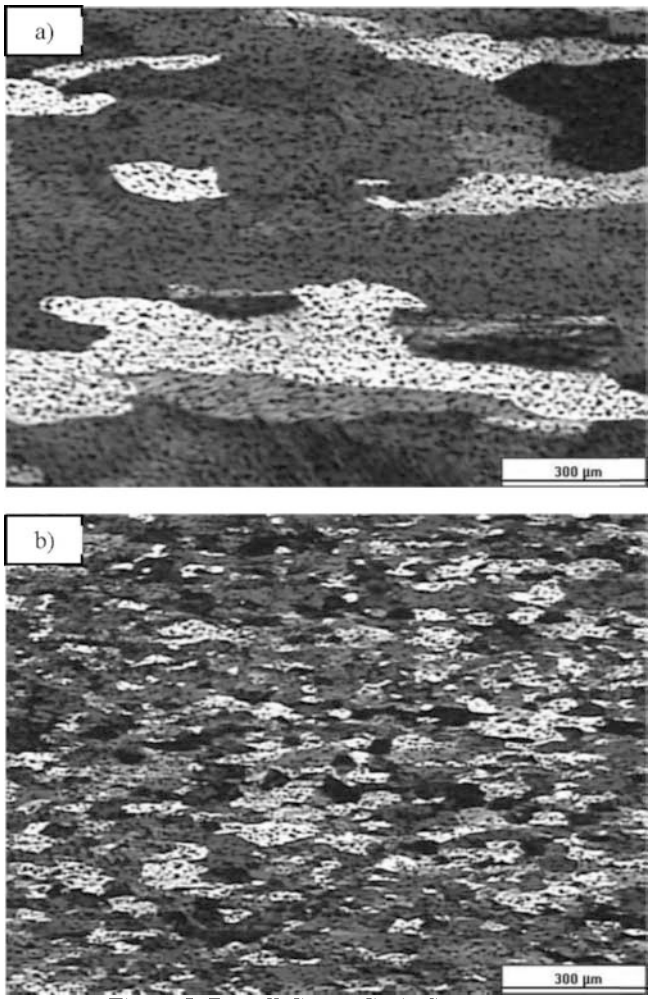

Figure 5: Re-roll Gauge Grain Structures

Scanning Transmission Electron Microscopy (STEM)

Samples for STEM analysis were prepared from sheets of the finish gauge for both alloys. The focus of the analysis was identifying the chemistries of the submicron precipitates and comparing the overall distribution of the precipitates. Figure 6a and b is set of STEM images of the precipitates observed for the S3xx4 and S3xx4V alloys, respectively. The overall precipitate distributions and sizes were similar for the two alloys. The thermodynamic calculations suggested the majority of the phases that would form are the same for the two alloys. The precipitates observed were primarily 100-200 nm in size. Accounting for the thickness contrast in the images, there were mainly two types of precipitates observed in the STEM analysis.

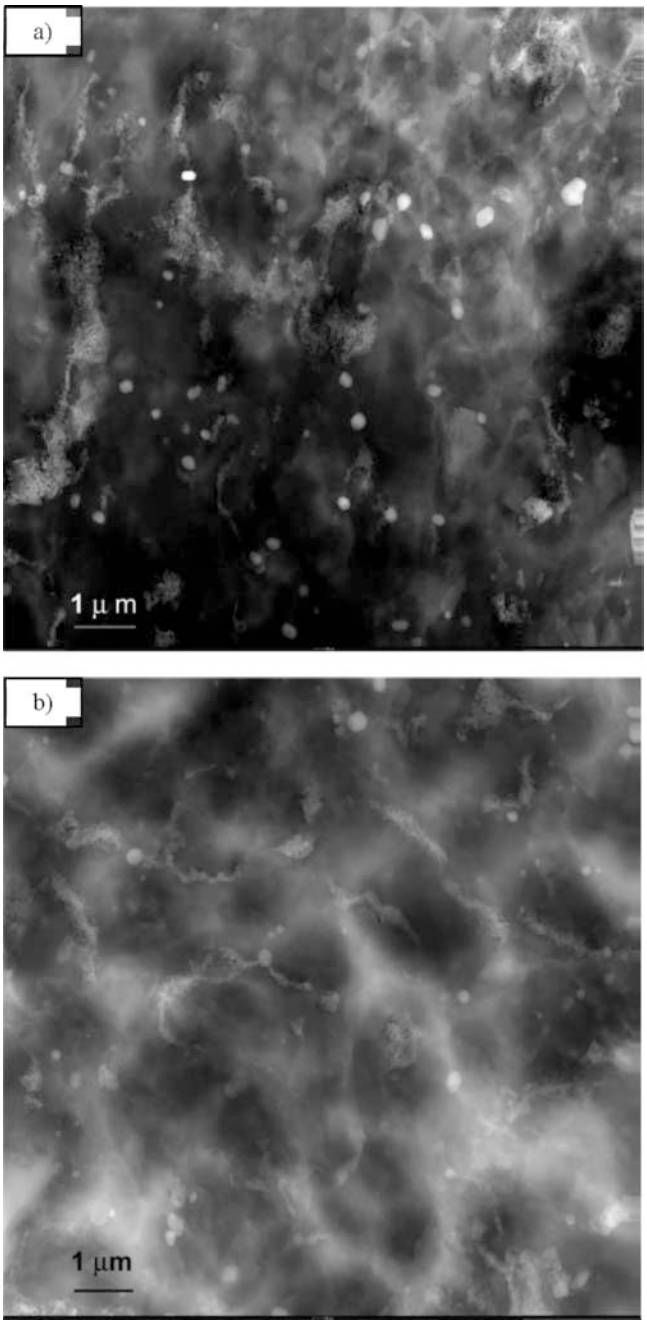

Figure 6: STEM Images of Sub Micron Particles

Figure 7 is a STEM image of two of the precipitates observed in the S3xx4 alloy. The two precipitates are both of the same phase; the brighter of the two, having a higher copper concentration. Copper can substitute in the lattice of three of Al-Fe-Mn phases indicated from the phase diagram which are the Al_3Fe, Al_6Mn, and Al(Fe,Mn)Si phases. The presence of Si in the EDS indicates the phase is Al(Fe,Mn)Si which was the predominant phase observed in the large constituent particles of figure 3 for both alloys.

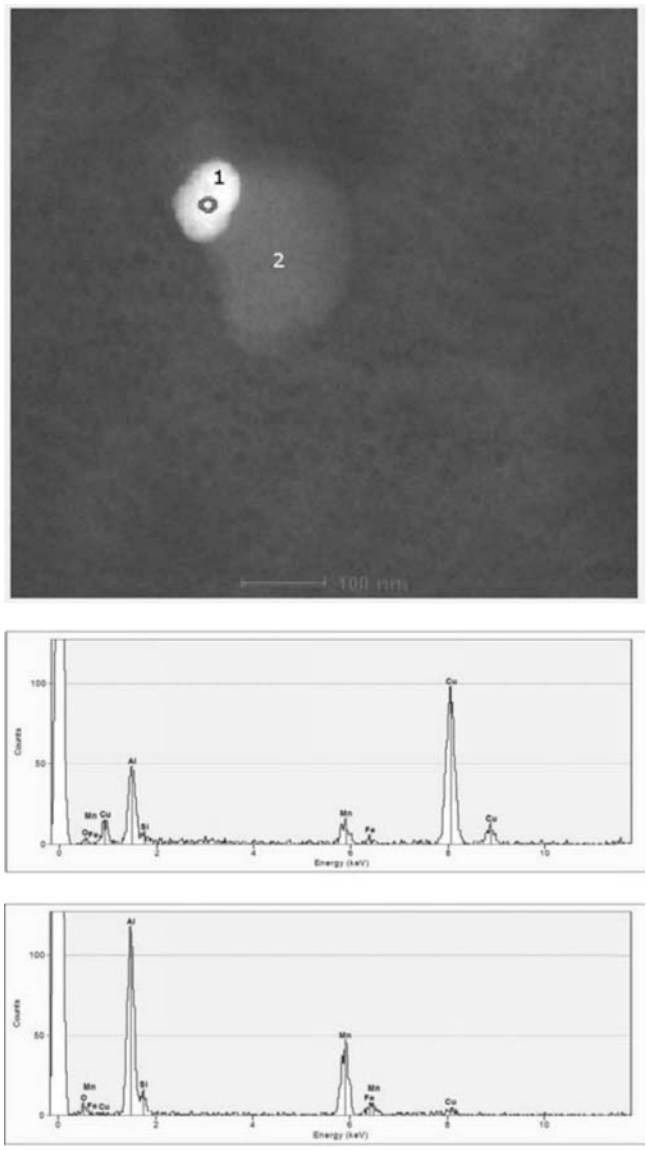

Figure 7: S3xx4 Precipitate STEM Image and EDS

Figure 8 shows the precipitates observed in the S3xx4V alloy and the EDS result for the precipitate marked with a red circle in the figure. The EDS indicated the presence of Al, Fe, Mn, Cu and V in the precipitate. The phases predicted to exist at equilibrium for which vanadium is present are the Al_3V, Al_3Fe, and the Al(Fe,Mn)Si. The existence of the Cu peak in the precipitate indicates the phase is likely the Al_3Fe phase and not the Al_3V phase. Cu is not a substitutional within the Al_3M phase (Al_3V). No precipitates were found that were consistent with the Al_3V phase without copper. Analysis of the diffraction pattern of the precipitate is needed to confirm the identity of the precipitates by lattice parameters and structure; however, based on the known information of the phase, it is likely to be the Al_3Fe phase with vanadium and copper as substitutional elements in the phase.

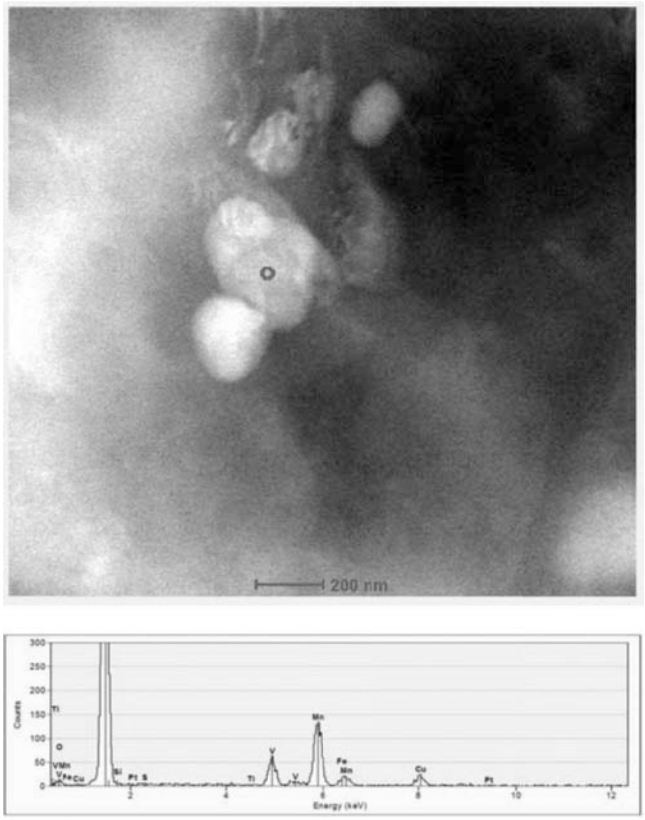

Figure 8: S3xx4V Precipitate STEM Image and EDS

Mechanical Properties

Mechanical testing of the re-roll and finish gauge samples showed the S3xx4V alloy had an increased yield strength and tensile strength with approximately the same elongation values. Figure 9a and b are the tensile and elongation results respectively for the two alloys at 0°, 45° and 90° to the rolling direction. Figure 10 is the tensile results for the two alloys at finish gauge along the 0°, 45° and 90° tensile directions. The tensile values were consistently 2 ksi higher for the S3xx4V alloy over the standard alloy with similar elongation values for both O-temper and H19-temper.

The difference of tensile strengths could originate from one of three possibilities – grain size, solid solution level, and precipitate structures. Grain sizes were observed to be smaller for the S3xx4V alloy and in other unpublished work, a higher solid solution level was indicated from resistivity measurements (6). Precipitation differences were not observed in the current study to be a factor.

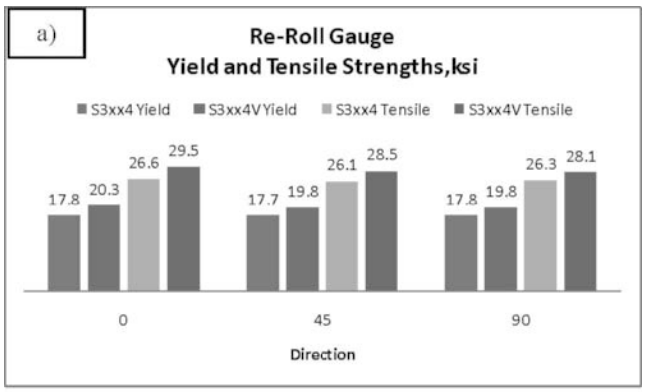

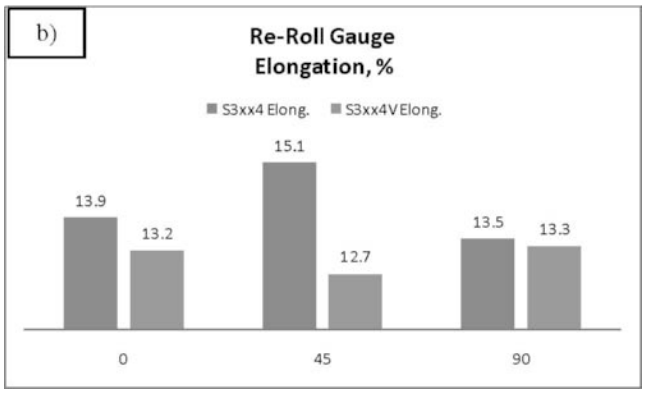

Figure 9: Re-Roll Gauge Tensile Results

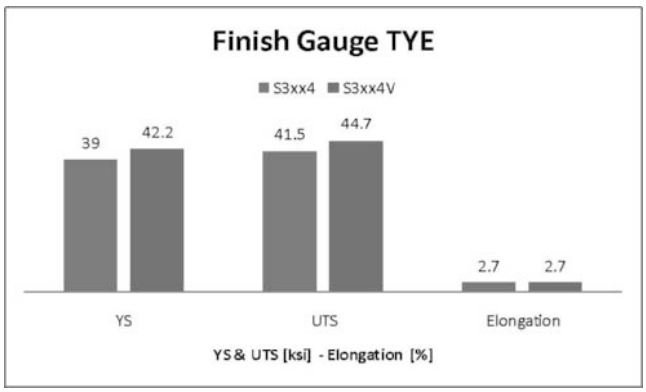

Figure 10: Finish Gauge Tensile Results

Conclusions

Based on analysis of the raw materials market and forward planning of expected trace element levels, a research program can be structured to systematically explore the consequence of particular trace elements at varying amounts. Internal specifications can be implemented in which more flexibility is allowed for off grade inputs. In the case study of increased vanadium in AA3xx4 alloy up to 0.10 wt. %, the following information was determined.

1. Vanadium would distribute within existing phases of the alloy
2. No changes to size or quantity are expected to occur in the constituent phases of the alloy over the base alloy
3. Potential additional phase Al_3V was not observed in STEM work
4. Grain structure of the re-roll gauge is refined with the vanadium introduction
5. Increases of vanadium resulted in a 2 ksi increase in mechanical properties at both O-temper and H19-temper without loss in ductility

References

1. **Das, S. K.** *Report 1-07-009.* Lexington, KY : Secat, Inc. Unpublished Internal Report.
2. **ASM International.** Section 4 Appendix. *ASM Handbook Volume 3 Alloy Phase Diagrams.* Materials Park, OH : ASM International, 1999.
3. **Westbrook, J. H. and Fleisher, R. L. Editors.** *Crystal Structures of Intermetallic Compounds.* New York, NY : John Wiley and Sons, 2000.
4. **Shi, P. and Sundman, B. Editors.** *TCC Thermo-Calc Users Guide Version S.* Stockholm, Sweden : STT and TCS, 2008.
5. **Lukas, H. L., Fries, S. G. and Sundman, B.** *Computational Thermodynamics - The Calphad Method.* New York, NY : Cambridge University Press, 2007.
6. **Yin, W.** *Report 1-06-014 Parts I-III.* Lexington, KY : Secat, Inc. Unpublished Internal Report.
7. **Totten, George and MacKenzie, D. Scott Editors.** *Handbook of Aluminum Volume 1 Physical Metallurgy and Processes.* New York, NY : Marcel Dekker, 2003.